THE AMERICAN SOCIETY OF MECHANICAL ENGINEERS
Three Park Avenue, New York, N.Y. 10016-5990

99-GT-208

Complementary Use of CFD and Experimental Measurements to Assess the Impact of Shrouded and Cantilevered Stators in Axial Compressors

M.S. Campobasso, A. Mattheiss, U. Wenger
Compressor Department EB1, BRR
BMW ROLLS-ROYCE
Dahlewitz, Germany

A. Amone, P. Boncinelli
"Sergio Stecco" Department of Energy Engineering
University of Florence
Florence, Italy

ABSTRACT

The performance of an axial compressor with either shrouded or cantilevered stators has been analyzed. The two configurations have been compared both at design and near stall operating conditions, with the aid of CFD and experimental measurements.

Results show that shrouded or cantilevered stators impact differently on the overall performance of the tested compressor. A higher stall margin occurs with the cantilevered build, while the work coefficient and the efficiency of the shrouded build at design conditions are higher.

An overall comparison of the shrouded and cantilevered design concepts has been carried out, not only in aerodynamic but also in economic terms.

NOMENCLATURE

$\dot{m}$	mass flow
p	static pressure
p_0	total pressure
T_0	inlet total temperature
β_{OV}	compressor pressure ratio
β_{ST}	stage pressure ratio
c_p	constant pressure specific heat
γ	specific heat ratio
c	absolute velocity
w	relative velocity
$c_{x,mid}$	axial velocity at midspan
u_{mid}	peripheral speed at midspan
ω	rotational speed
$\mathcal{T}$	measured torque
η_m	mechanical efficiency
$\Delta\mathcal{L}$	computed angular momentum variation between stage outlet and inlet
$\overline{p}_1$	pitchwise area averaged static pressure at rotor/stator inlet
$\overline{p}_{01(2)}$	pitchwise area averaged relative total pressure at rotor/stator inlet (outlet)
$\alpha = \tan\frac{w_u}{w_x}$	pitchwise area averaged rotor flow angle
$\alpha = \tan\frac{c_u}{c_x}$	pitchwise area averaged stator flow angle
$C_p = \frac{p-\overline{p}_{1,MID}}{(\overline{p}_{01}-\overline{p}_1)_{MID}}$	static pressure coefficient
$C_{p_0} = \frac{\overline{p}_{01,MID}-p_0}{(\overline{p}_{01}-\overline{p}_1)_{MID}}$	total pressure coefficient
$\Omega = \frac{\overline{p}_{01}-\overline{p}_{02}}{(\overline{p}_{01}-\overline{p}_1)_{MID}}$	loss coefficient
$\phi = \frac{c_{x,mid}}{u_{mid}}$	flow coefficient

Presented at the International Gas Turbine & Aeroengine Congress & Exhibition
Indianapolis, Indiana — June 7–June 10, 1999

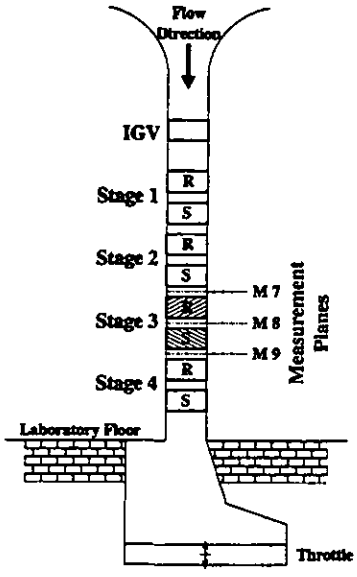

Figure 1: Sketch of the Test Facility.

$$\psi_{is,ST} = \frac{c_p T_0 \left(\beta_{ST}^{\frac{\gamma-1}{\gamma}} - 1 \right)}{u_{mid}^2/2}$$ stage isentropic work coefficient

$$\psi_{is,OV} = \frac{1}{4} \frac{c_p T_0 \left(\beta_{OV}^{\frac{\gamma-1}{\gamma}} - 1 \right)}{u_{mid}^2/2}$$ compressor isentropic work coefficient

$$\eta_s = \frac{c_p T_0 \dot{m} \left(\beta^{\frac{\gamma-1}{\gamma}} - 1 \right)}{\Delta \mathcal{L}}$$ stage efficiency

$$\eta_c = \frac{c_p T_0 \dot{m} \left(\beta^{\frac{\gamma-1}{\gamma}} - 1 \right)}{\eta_m \mathcal{T} \omega}$$ compressor efficiency

INTRODUCTION

The efficiency of gas turbine components has experienced remarkable improvements over the last 30 years (e.g. Wisler, 1998). Nowadays industries and research centers orient their research activities to the investigation and understanding of complex loss mechanisms whose comprehension could help improve the performance of the new generation of turbomachinery.

Leakage flows in axial compressors belong to this category, as the associated loss can considerably spoil the performance. Its reduction depends on the aerodynamic design, the construction features and the mechanical state (e.g. frettage and small plastic deformations). For instance, the leakage mass flow through the gap between the rotor blade root and the disc slot is likely to be higher with axial roots rather than with circumferential dovetails, since the axial slots in the discs are aligned with the main stream, while the circumferential groove housing the dovetails is perpendicular to it. In both cases, the amount of leaking mass flow also depends on the pressure rise across the rotor and the effectiveness of the sealing devices. Despite the aerodynamic advantage of circumferential dovetails, more constraining mechanical issues often oblige one to choose axial roots.

The loss that arises from the leakage of flow over the tip of rotor blades and from the hub clearance of stator vanes has undergone more systematic investigation. Specific loss mechanisms clearly depend on whether the blades are shrouded or cantilevered.

Axial compressor rotor blades are typically cantilevered. The aerodynamic performance decrease caused by rotor tip leakage flows and its dependency on the radial gap width have been experimentally investigated both in an isolated compressor stage (Goto, 1991) and in a four–stage low– speed axial compressor (Howard et al., 1994). Howard et al. (1994) shows that increasing the radial gap between rotor tips and casing from 1.2% of the blade height to 3% leads to a stage efficiency drop, 30% of which is due to stator loss and 70% to rotor loss. This points out how leakage flow does not affect merely the flow field in the blade row where it arises, but also the adjacent ones.

In the design of stator vanes, designers can examine both the shrouded and the cantilevered hub solutions. The shrouded–stator style is more widespread than the cantilevered one, but nonetheless there are recent examples of aeronautical HP compressors having cantilevered stators in the rear stages. Non–aerodynamic factors like costs, weight, reliability and overall design of the compressor affect the choice of the design. On the aerodynamic side, the choice to shroud eliminates the troubles associated with hub leakage, but replaces them with the difficulties of shrouded stator leakage, in which flow normally recirculates backwards through the cavity between the stator shroud–box and the rotor arm. Leakage flow in shrouded stators of axial compressors has recently been the object of accurate numerical and experimental investigation. Heidegger et al. (1996) published the results of a numerical study on the interaction between main stream and seal cavity leakage flow in an isolated stator and on its dependency on the geometry of the cavity. Two years later, Wellborn and Okiishi (1998) assessed the impact of this loss source in the multistage environment, by means of flow field measurements in a low–speed four–stage compressor and single row numerical computations of the flow field in the third stator. Their results reveal that for every 1% increase in seal–tooth clearance–to–span ratio, the pressure rise penalty is nearly 3%, while efficiency drops 1%.

Using measured data in the third stage of a four–stage low–speed compressor, Swoboda et al. (1998) compared the aerodynamic performance of two compressors differing only in the stator hub build: cantilevered or shrouded. Overall performance analysis shows slightly higher work coefficients for shrouded stators, but slightly higher stall margins for the cantilevered compressor.

It has been shown (Howard et al., 1994, Wellborn and Okiishi, 1998) that leakage in one blade row affects both the flow field in the blade where it originates as well as the downstream rows. As a consequence, the performance of each row also depends on the sealing design of the previous ones. In order to optimize compressor design, these interactions and their effects on the aerodynamic characteristics of the whole compressor should

be taken into account. This would provide useful data for the choice of the stator–hub set–up and allow one to improve the aerodynamic design of both stator and rotor hub sections. These phenomena, however, are not exhaustively modeled in classical design tools like through–flow and blade–to–blade approaches. On the contrary, three–dimensional multistage Navier–Stokes solvers can have the capability of dealing with the issue. The present work was conceived 1) to compare the aerodynamics of shrouded and cantilevered stators in an axial compressor, 2) to prove the capability of CFD of predicting flow changes between adjacent rows and overall performance variations at the stage level due to leakage, 3) to provide information on the flow field not easily attainable with measurement techniques in the multistage environment (e.g. flow visualization on blade surfaces), and 4) to discuss the choice of shrouded/cantilevered stators in the light of mechanical, economic and weight reduction issues.

The first objective was accomplished by means of experimental measurements in a four–stage low–speed axial compressor. Two compressor configurations were investigated: the former with all four stators equipped with a shrouding ring (build 1) and the latter with all four stators cantilevered (build 2). For the remaining aerodynamic and mechanical attributes, build 1 and build 2 were identical.

A three–dimensional multistage incompressible Navier–Stokes solver (HYDRO) was used to pursue the second objective, with one– and multi–row computations of the flow fields in the build 1 and build 2 compressor. The flow field of the coupled second and third stages at design conditions was analyzed to account for the impact of changes in the hub geometry on both rotors and stators. Single row computations were performed near stall, where blade row interactions are strong and cannot be resolved satisfactorily using the mixing plane formulation implemented in the solver.

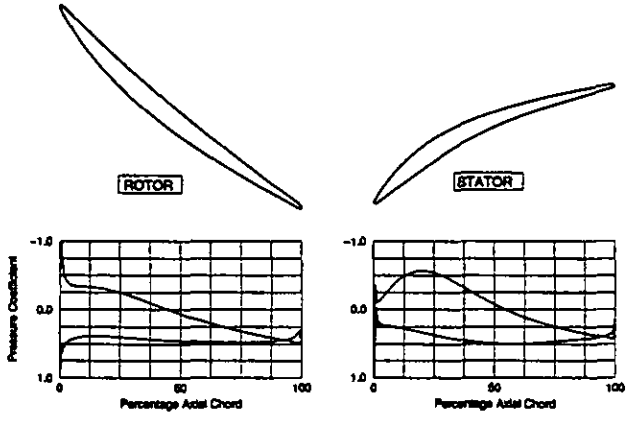

Figure 2: Rotor and stator profiles at midspan and their typical loading distributions at design operating conditions.

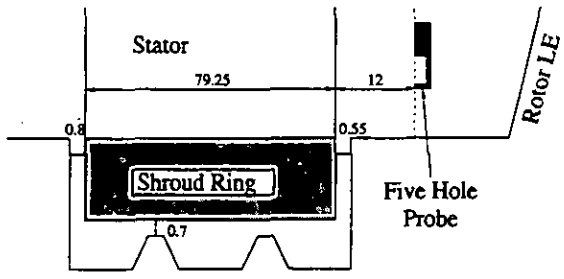

Figure 3: Build 1 shroud box, sealing and gap sizes (measures in *mm*).

TEST FACILITY, INSTRUMENTATION AND COMPRESSOR DESIGN

The four stage Low–Speed Research Compressor (LSRC) at the Technical University of Dresden (Germany) was used for the experimental investigation. The test facility is sketched in Fig. 1 and its description is provided in DUT (1997).

The detailed performance of the third stage rotor and stator was investigated by means of measurements in the absolute frame using a traversing five–hole probe and a boundary layer probe. In this way planar mappings and pitchwise averaged radial distributions of static and total pressure, pitch and yaw angle were obtained at rotor inlet, stator inlet and stator outlet.

Static pressure taps, located in a matrix of circumferential and radial positions on the vane and blade surfaces provided airfoil pressure distribution and loading. Both endwalls were also instrumented with pressure taps.

Overall performance is based upon measured airflow, measured work input (torque and speed) and measured pressure rise.

All pressures were measured on pressure transducers having an accuracy of ±0.015%. Overall measurement accuracies are as follows: mass flow and pressure ratio are accurate to within ±0.37% and ±0.02% respectively and efficiency is accurate to within ±0.9 %.

Two configurations of the compressor were tested, differing only in the stators hub: with all stators shrouded (build 1) or with all stators cantilevered (build 2).

The common platform is an axial machine with four equal stages, designed to be representative of the rear stages of a modern high pressure compressor.

Rotor and stator profiles at midspan and their typical loading distributions at design operating conditions are shown in Fig. 2. The presence of a spike at rotor leading edge shows that incidence to the rotor is quite high even at design operating conditions. Table 1 provides the main geometric data and aerodynamic attributes of the tested compressor.

The (build 1) shroud box, its sealing and the gap sizes are represented in Fig. 3. The seal tooth clearance , the leading edge and the trailing edge axial gaps correspond respectively to 0.58%, 0.67% and 0.46% of blade height. It should be noticed that in real compressors, the axial gaps between the shroud and the rotor rims are considerably higher than those shown in Fig. 3,

Compressor Data	Rotational Speed	1000 RPM
	Annulus Outer Diameter d_{out}	1500 mm
	Annulus Inner Diameter d_{in}	1260 mm
	Annulus height h	120 mm
	Mass Flow	25.2 Kg/s
	Pressure Ratio	1.106
	Flow Coefficient ϕ	0.53
	Compressor Loading $\psi_{is,OV}$	0.8
	Degree of Reaction	0.65
Rotor	Number of Blades	63
	Camber (Midspan)	22.13°
	Stagger Angle (Midspan)	40.84°
	Pitch to Chord (Midspan)	0.624
	Aspect Ratio (Midspan)	1.088
	Radial Clearance ($clrt/h$)	1.25%
	Diffusion Factor	0.431
	Reynolds Number	5.6 10^5
Stator	Number of Blades	83
	Camber (Midspan)	41.50°
	Stagger Angle (Midspan)	25.29°
	Pitch to Chord (Midspan)	0.587
	Aspect Ratio (Midspan)	1.349
	Radial Clearance ($clst/h$)	1.5%
	Diffusion Factor	0.413
	Reynolds Number	3.5 10^5

TABLE 1: Main geometric data and aerodynamic attributes of the tested compressor at design conditions.

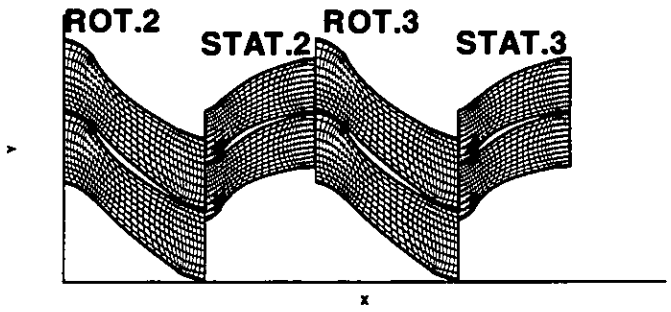

(a) Blade–to–blade section of the computational grid.

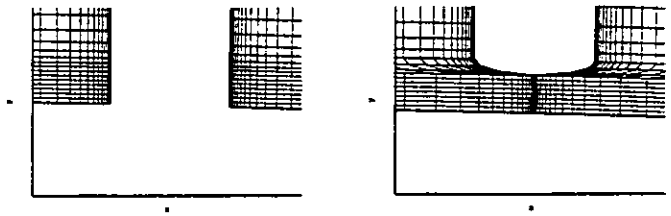

(b) Clearance periodic and blade–tapered models.

Figure 4: Details of the computational grid and clearance model.

sometimes up to 10% of the stator hub chord. The possible impacts of this difference on the performance of the build will be discussed later.

MULTISTAGE NS SOLVER, GRIDS AND PRELIMINARY ANALYSIS

Computed results were obtained using the HYDRO code which is an incompressible version of the TRAF code, a 3D fully–viscous, stationary, multigrid, multirow code for blade row analysis. Coupling between rows is achieved by using mixing planes, which are handled by keeping the radial distribution of physical quantities while averaging in the circumferential direction (*"pitch averaging"*). Further details on the numerical procedure can be found in Arnone et al. (1993), Arnone and Benvenuti (1994) and Arnone and Pacciani (1995).

For both rotor and stator blades, a periodic H–type grid was used with 133 mesh points in the streamwise, 45 in the pitchwise and 49 in the spanwise direction, for a total of 278,784 computational cells per row. About 1000 iterations were necessary for full convergence (machine accuracy, single precision) on this mesh and this required about 8 hours per row on a 195 Mhz R10000 SGI Origin. With the chosen minimum spacings, y^+ varied between 1 and 4. In fig. 4(a) a schematic view of the grid for stages 2 and 3 is shown, with only some of the mesh points being illustrated for clarity's sake.

Neither the shrouded stator seal cavities nor the leakage flow were modeled and the relevance of this approximation on the conclusions derived from this study will be discussed later. Radial gaps of cantilevered blade rows (all rotors and build 2 stators) could be modeled either with a full–span blade and periodic boundary conditions on the cell faces adjacent to the radial gap or with a tapered blade (Fig. 4(b)), with the hub rotating in both cases. The latter model reproduces the measured loss contours at stator exit better, while the former underestimates the measured leakage loss. Consequently the tapered blade model was adopted.

To assess the independence of the solution on further mesh refinement, the flow field in the cantilevered stator and the rotor were computed both with the $133 \times 45 \times 49$ mesh (278,784 cells) and with a $212 \times 72 \times 80$ mesh (1,221,120 cells). The observed differences were small (see Fig. 5(a)–5(b)), and were judged negligible for the purposes of the study and the $133 \times 45 \times 49$ mesh was used throughout the analysis.

OVERALL PERFORMANCE

The measured overall performance of the compressor with shrouded stators (build 1) and with cantilevered stators (build 2) is presented in Fig. 6(a). At design conditions, both the work coefficient and the efficiency of the shrouded compressor are about two points above those of the cantilevered one. As the load in-

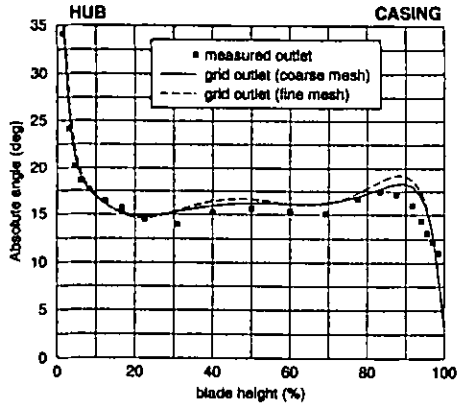

(a) Pitch angle α at the cantilevered stator outlet.

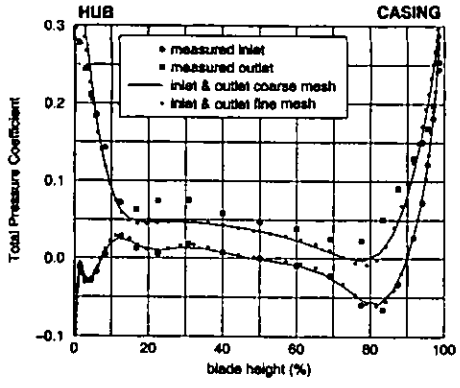

(b) Total Pressure Coefficient C_{p0} at the cantilevered stator inlet and outlet.

Figure 5: Comparison between coarse and fine meshes for the third stage cantilevered stator at design conditions.

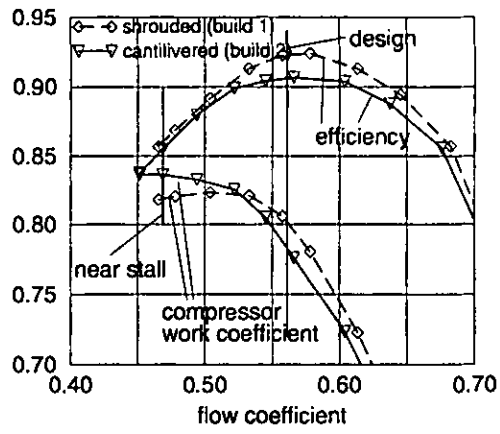

(a) Compressor overall performance

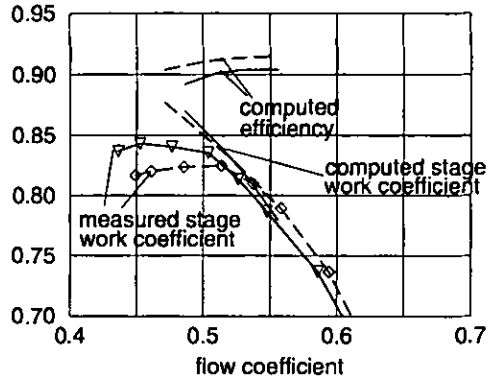

(b) Stage III performance

Figure 6: Computed and measured performance of the tested compressor.

creases, these trends gradually reverse, until at "near stall condition" (Fig. 6(a)), the efficiency of the shrouded compressor is only 0.5% higher than the cantilevered one, which has a higher work coefficient (about two points more than the shrouded one). The minimum mass flow corresponds to the stall inception and the cantilevered compressor has a lower value of this parameter. This analysis shows that the shrouded compressor performs better around the peak efficiency conditions and the cantilevered one has a higher stall margin.

The uncertainty margin affecting the measurements could make one douht these statements. Because of the $\pm 0.9\%$ accuracy on the efficiency determination, the observed difference of ± 2 points at design conditions, could reduce to 0.4 in the worst case. In order to further investigate this question, one-stage computations of the flow field in the third stage of both huilds were carried out. For hoth huilds, rotor 3 inlet boundary conditions at design point and near stall were imposed using the corresponding measured profiles of total pressure and pitch angle. At the outlet, static pressure at the hub was imposed and spanwise static pressure distribution was extrapolated by means of radial equilihrium concept, in order to adjust the mass flow. For all operating points, differences between measured and computed mass flow were kept within 0.5%. For the computed operating points hetween design and near stall ones, the inlet houndary conditions were interpolated.

Figure 6(b) provides the computed efficiency, and the measured and computed work coefficient curves of the third stage. At design conditions, measured and computed work coefficient are in a gond agreement. A measured difference of about 2 points corresponds to a computed one of 1.5. The computed difference in stage efficiency is 1.1 points. As the load increases, the agreement between measured and computed work coefficient of the third stage worsens, where the calculations overestimate the

measurements. This effect could be explained as due to strong blade row interactions not adequately modeled by the mixing plane approach. At design loading such interactions are weaker, and the model worked properly. This is proved also by the fact that the differences in the computed performance of the third stage at design mass flow are consistent with those in the measured performance of the overall compressor.

DESIGN OPERATING CONDITIONS

A detailed analysis of the flow field in tbe third stage at design conditions was carried out with the aid of measured and computed results. Simulations of the flow field in the isolated rotor and stator of both the shrouded and cantilevered stage were performed using measured radial profiles of total pressure and pitch angle to implement inlet boundary conditions. Their purpose was to clarify the different loss mechanisms induced by the stator hub geometry. Successively, quantitative flow differences were assessed by comparing measured data to results of multistage calculations (second and third stages) for both the shrouded and cantilevered compressors. Once again, the inlet flow field at the second rotor was taken from experiments in the shrouded compressor. Although the investigation was focused only on the third stage, the second one was also included in the calculations, in order to account for the effect of the stator hub type at the third rotor inlet. Measured contours of total pressure coefficient at cantilevered and shrouded stator outlet are compared with single row calculations in Fig. 7. Computed and measured contours at the same axial location are in a relatively good qualitative and quantitative agreement. The main difference between the two stators occurs near the hub. The bubble–shaped area of low total pressure near the hub of the cantilevered stator corresponds to the loss produced by the leakage flow between the stator tip and the rotating hub. A smaller but denser loss region is visible at the hub of the shrouded stator. The loss generation mechanism causing the low pressure area near the casing appears to be the same in the shrouded and cantilevered stator, as both experimental and computed contours have similar shapes and levels.

Figure 8 shows flow visualizations on rotor and stator suction sides obtained with isolated row calculations. Axial and radial velocity components in the first mesh surface after the blade suction side were used to draw these quasi skin friction lines. The hub corner separation on the suction side of the rotor is larger when the rotor is emhedded in the cantilevered stage. No corner separation is visible in the tip region of either rotors. This is due to the rotor tip leakage jet. Fluid particles near the suction side deviate from the axial direction towards the tip and join the leakage jet as soon as it comes out from the radial gap. This motion is the opposite of the one that a passage vortex would induce therefore reducing tendency to tip corner separation. For the same reason, no hub corner separation is visible near the hub of the cantilevered stator. Conversely, typical corner stall patterns are present at the hub of the shrouded and at the casing of both stators.

Computed and measured differences of incidence, deviation, turning and loss for the third stage rotors and stators

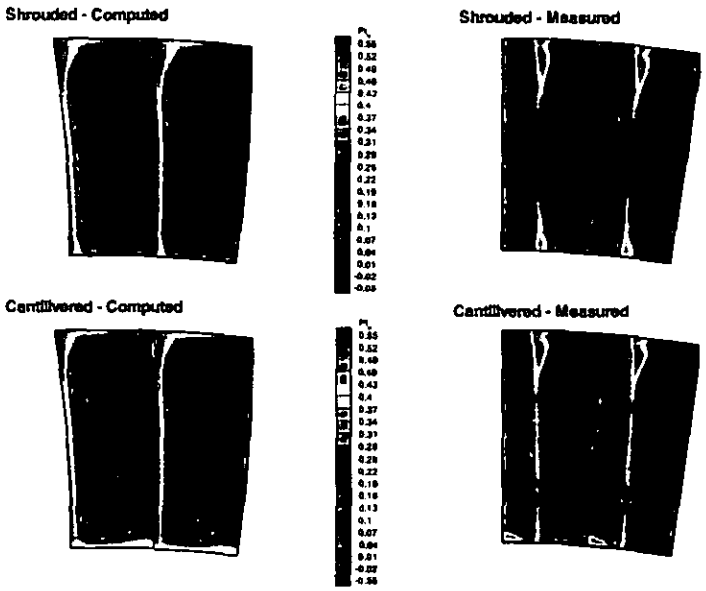

Figure 7: Computed and measured contours of total pressure coefficient at shrouded and cantilevered stator outlet (design conditions).

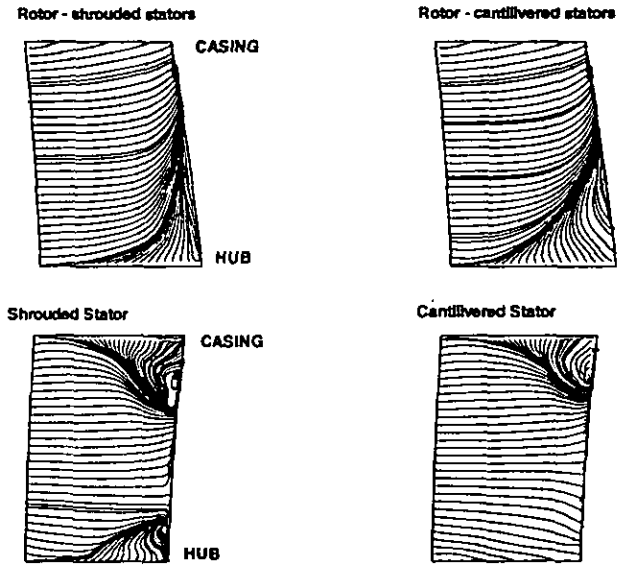

Figure 8: Flow visualizations on rotor and stator suction sides from isolated row calculations (design conditions) using measured data as inlet boundary conditions.

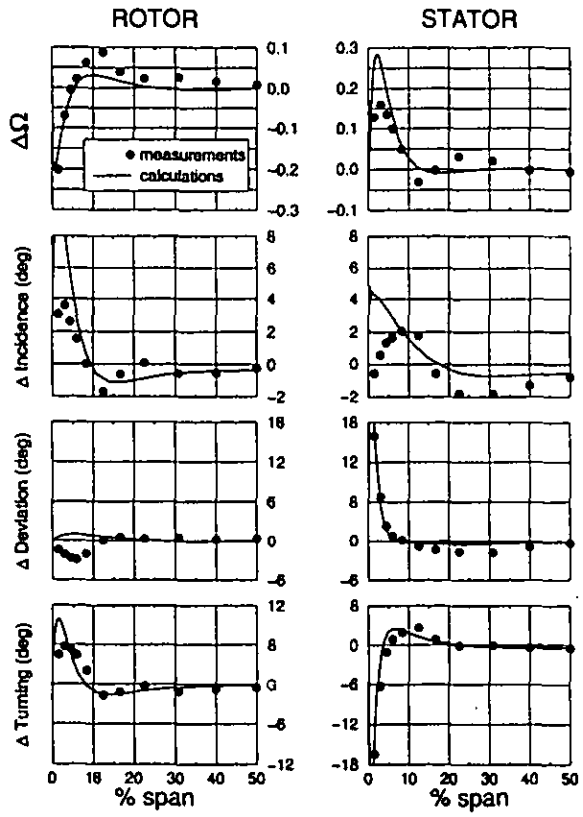

Figure 9: Computed and measured differences of losses, incidence, deviation and turning for the third stage rotors and stators between cantilevered and shrouded builds (Δ = cantilevered – shrouded quantities).

are shown in Fig. 9. Computed results refer to the two-stage calculations with coupled second and third stages. Profiles are calculated subtracting pitchwise area averaged flow quantities of the shrouded compressor from those of the cantilevered one (Δ = cantilevered – shrouded quantities) and plotted from hub to midspan. Differences from midspan to casing are considerably smaller. Both measurements and calculations reveal that incidence of the third rotor embedded in the cantilevered compressor increases from the hub to 10% of the blade height. This increases the corner stall on the suction side of this rotor, as observed in the particle traces plots. The higher incidence increases the loading of the hub sections and possibly causes a stronger hub passage vortex visible in the spanwise rotor loss variation. The low energy fluid of the hub boundary layer is swept towards midspan faster along the suction side and replaced by free stream material with higher energy content. This phenomenon is reflected in the lower loss in the first 5% of the blade height and in the higher loss from 5 to 15% of the blade height. Incidence and deviation of the third stator also increases near the hub in the cantilevered compressor. The computed peak of incidence variation of about 4 degrees occurs almost at the hub, while the measured peak of 2 degrees occurs at 10% of the blade height. Deviation of the cantilevered stator is up to 16 degrees higher near the hub. Calculations with rotating and stationary hub pointed out that this is mainly due to the hub leakage jet

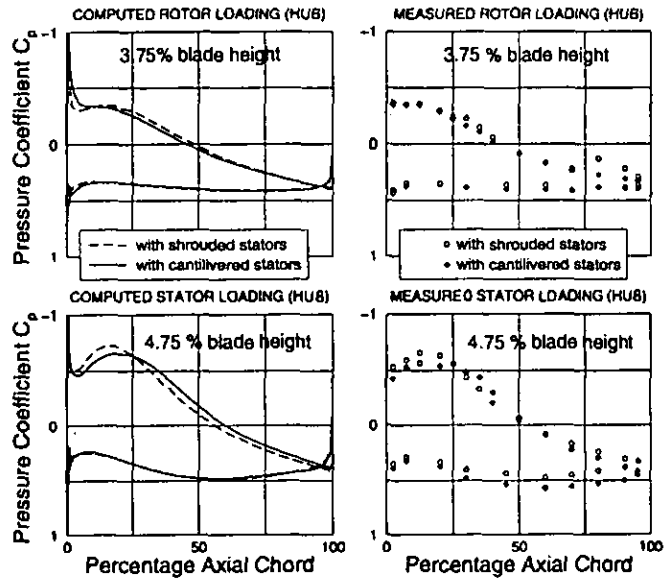

Figure 10: Computed (multistage) and measured static pressure coefficient C_p on rotor and stator blade near hub (design conditions).

and only marginally to the hub rotation. Both measurements and computed results exhibit higher losses in the first 10% of the blade height in the cantilevered stator. This means that, at design conditions, the loss produced by the hub leakage of the cantilevered stator is higher than the one associated with the hub corner stall of the shrouded stator. This is believed to be the main reason why at design conditions the shrouded compressor has higher efficiency, since measurements and calculations show minor variations in the rotor losses.

Computed (multistage) and measured static pressure distributions on rotor and stator blade near hub are in good agreement as depicted in Fig. 10. Rotors embedded in the cantilevered compressor are slightly more loaded because of the incidence increase. The shrouded stator loading is slightly higher and the minimum peak pressure is shifted forward, despite the higher incidence in the cantilevered one. This inconsistency is only apparent because the leakage flow alters the flow field in a highly three-dimensional manner, involving alterations of the radial velocity field.

NEAR STALL OPERATING CONDITIONS

Investigation on the third stage flow field near stall was carried out mainly with the aid of measured data and results of numerical single row computations. Measured data were used to set the row inlet boundary conditions. Two-stage calculations based on a mixing plane approach did not provide satisfactory results, probably because of the strong unsteady interactions in the presence of large regions of separated flow, which have been experimentally observed at these high loading working conditions.

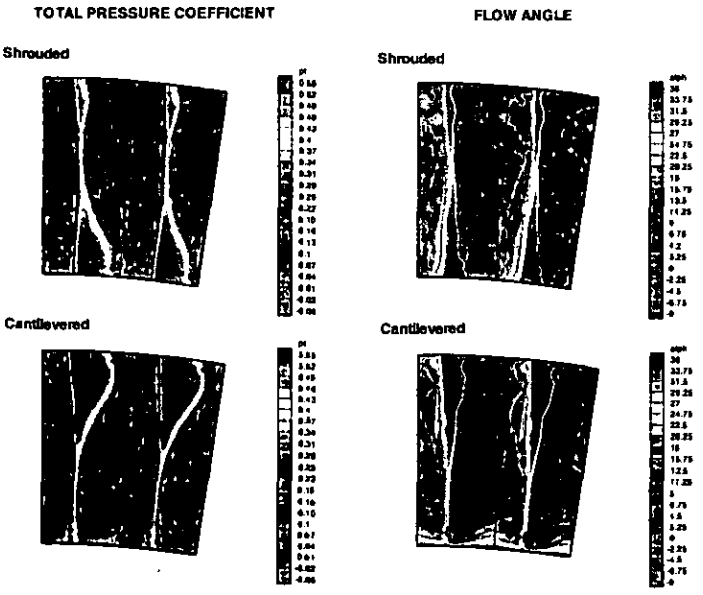

Figure 11: Measured contours of total pressure coefficient C_{p0} and pitch angle α at shrouded and cantilevered stator outlet (near stall conditions).

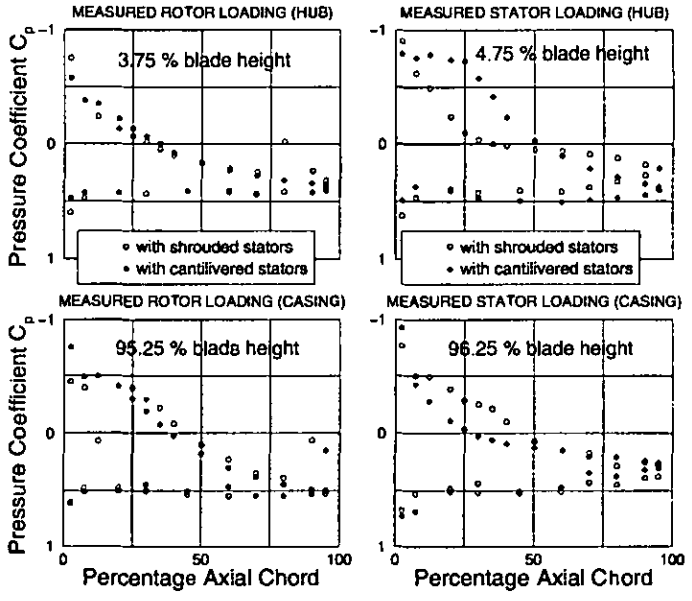

Figure 12: Measured static pressure coefficient C_p on rotor and stator blade near endwalls (near stall conditions).

Figure 11 shows the measured contours of the total pressure coefficient and the pitch angle at the stator exit. At the hub, the large high–loss area of the shrouded stator is caused by a strong corner stall and the remarkably smaller loss region of the cantilevered stator is due to the leakage flow. At the casing, the corner stall loss of the cantilevered stator is much greater than that of the shrouded one. This could be due to the fact that the hub corner separation in the shrouded stator increases the blockage in that region, and consequently the flow is diverted outward towards the casing. This effect reduces the diffusion near the casing, thereby decreasing the size of the casing corner separation in the shrouded stator. It should be noted how this loss distribution is different from the one at design conditions, where losses at the shrouded hub were lower and similar losses occur at the casings of both stators.

Flow angle contours also point out had flow conditions near the casing of the cantilevered stator and near the hub of the shrouded one. In the red triangular areas, the value of exit pitch angle α is higher than 36 degrees. This is due to the lower axial velocity, caused by recirculations near endwalls. Just as in design conditions, the leakage jet at the hub causes a strip–shaped region of high exit flow angle.

Measured blade loadings near the endwalls are compared in Fig. 12. Static pressure profiles of the shrouded compressor rotor are slightly more loaded near the hub, in the first 10 % of the blade chord, while the loading of the third cantilevered compressor rotor is higher near the blade tip, in the first 20% of the blade chord. The flat pressure distribution on the suction side of the shrouded stator near the hub and of the cantilevered

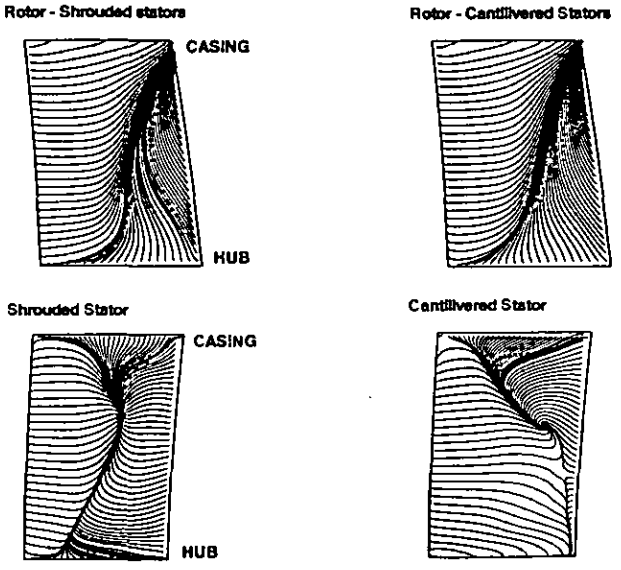

Figure 13: Flow visualizations on rotor and stator suction sides from isolated row calculations (near stall conditions).

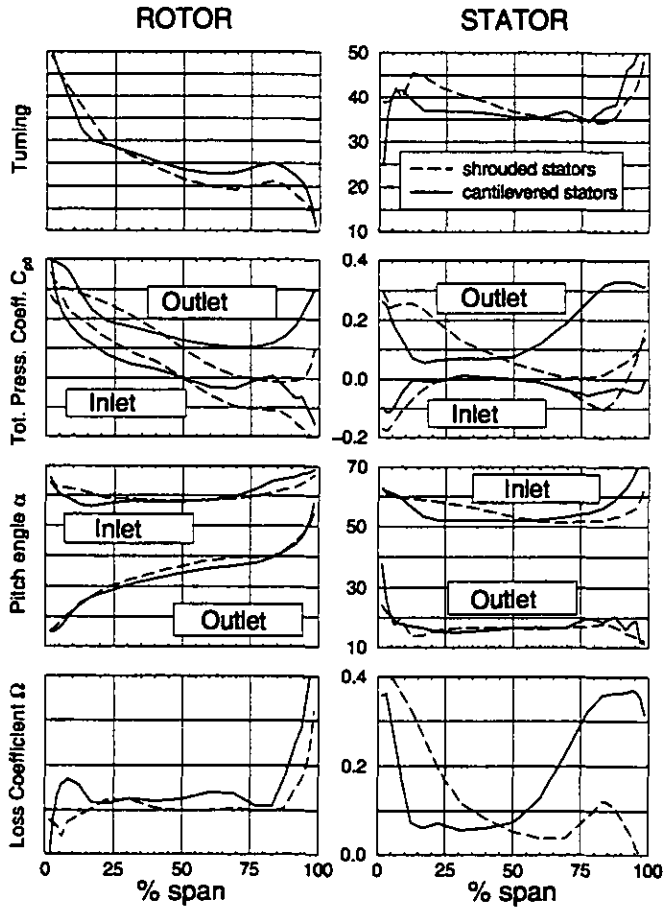

Figure 14: Measured turning, total pressure coefficient C_{p_0}, pitch angles α and losses Ω in the third stage for both stator configurations.

stator near the casing demonstrates the separated flow at these positions.

Numerical flow visualizations on the rotor and on the stator suction side are shown in Fig. 13. The hub corner stall is slightly larger in the cantilevered compressor rotor. In the gap region near the trailing edge, the quasi skin–friction lines deviate faster towards the tip clearance, pointing out a stronger leakage flow. Comparing stator suction sides proves again how the hub leakage flow prevents the hub sections from stalling, just as at design conditions: while the flow separates from hub to casing on the suction side of the shrouded stator, neither large regions of reverse flow nor any trace of a corner stall are visible in the cantilevered stator hub. However, the flow near the casing has worsened, because the corner stall extends further upstream.

Figure 14 shows measured losses and turning in the third stage. Sharper relative total pressure and pitch angle spanwise gradients are observed near hub at the inlet plane of the cantilevered compressor rotor. These strengthen the hub passage vortex and the corner stall, as seen in the flow visualizations.

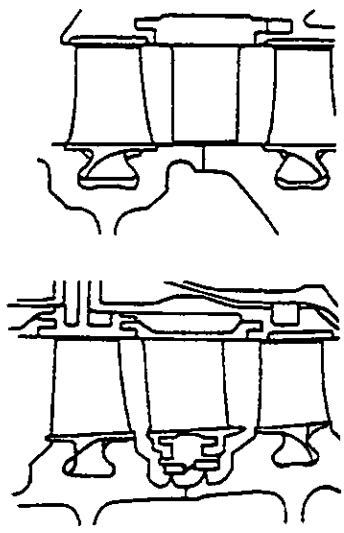

Figure 15: Schematic lateral view of cantilevered and shrouded stator hub of a real axial compressor.

The rotor loss profile distribution evidences a higher loss up to 20% of the blade span. From 75% span to casing, the rotor inlet flow angle is between 2 and 5 degrees higher with cantilevered stators. This higher incidence increases the loading of the tip section and the leakage mass flow, causing higher losses from about 80% of the span to the casing.

Larger differences occur in the stators. Losses are higher at the shrouded stator hub and at the cantilevered stator casing. Maximum losses at both endwalls correspond to corner separations, that increase blockage. The consequent reduction in axial velocity causes the incidence to increase. This explains why the inlet angle is up to 10 degrees higher from 75% of the blade span to the casing in the cantilevered stator case and up to 6 degrees higher from midspan to hub in the shrouded stator case.

The overall losses of both stators are similar, and the cantilevered compressor rotor has a slightly higher loss all over the blade span. This is consistent with experimental observation that even at near stall conditions the shrouded compressor has higher efficiency, although the difference is lower than at design conditions.

DISCUSSION OF RESULTS AND NON–AERODYNAMIC CONSIDERATIONS

It has been shown why the shrouded compressor used in this investigation performs better than the cantilevered one at design conditions and why the cantilevered one performs better as one moves towards stall conditions.

However, as it was noticed earlier, in this case the axial gaps between the shroud and the rotor rims are considerably smaller than those in real compressors. Consequently it is quite likely that the associated leakage flow had a very small disturbance

action on the main flow of the shrouded compressor, remarkably weaker than that one occurring in a real machine. This circumstance could explain the contradiction between the higher efficiency of the shrouded build at design operating conditions found in the present analysis and the slightly higher efficiency of the cantilevered compressor found in Swoboda et al. (1998), where the above–mentioned axial gaps were about ten times larger than those of the shrouded compressor used for the present investigations. In the case under investigation, not modeling the leakage flow in the shrouded build should not affect the results of the computations in a significant way. On the other hand, the work of Swoboda et al. (1998) also found that the cantilevered stator compressor had higher stall margin than the shrouded one, showing that this feature does not depend primary on the axial gap width.

The detached flow at the hub of the shrouded stator and its absence in the cantilevered stator were also observed in the third stator of a four stage low–speed research compressor (Brankiewicz and Hathaway, 1998), indicating that also this difference between shrouded and cantilevered stators is not primary affected by the axial gap geometry.

A schematic lateral view of cantilevered and shrouded stator hub of a real axial compressor are shown in Fig. 15. Quite often, the choice of the stator hub depends on mechanical constraints. Modern axial compressors have typically welded rotors. In this case, cantilevered stators cannot be used if the roots of the upstream and downstream rotor are axial, because disc spacers must be below the annulus inner wall to allow both the broaching tool and rotor roots to enter the axial disc slots.

Efforts to develop small engines with cantilevered stators may be greater than those with shrouded stators, as the hub clearances of the former ones may need to be increased to take into account deflections, mechanical and thermal transients, etc. This may also result in more opened clearances for cantilevered stators by the time the engine is actually fielded. However recent cantilevered stator designs of larger civil engines with *independent full ring casings* (passive clearance control) gave good thermal matching and good clearance control of cantilevered stators and rotors, without obliging one to increase radial clearances to achieve it.

Component	Cantilevered	Shrouded
Vane	datum	+ 9%
Shroud		+ 3%
Rotor disc–Spacers	datum	slightly more
Total	**DATUM**	+ 12%

TABLE 2: Comparison between cantilevered and shrouded stators in terms of stage cost.

Table 2 shows a comparison between cantilevered and shrouded stators in terms of stage cost. The term "vane" includes the stator airfoil, the outer platform, holding the stator blade at the casing and the inner platform. The shroud is normally a junction element (e.g. ring) passing through all the inner platforms and keeping them together. Because of the inner platforms and the shrouding ring, the shrouded stator stage can cost about 10% more than the cantilevered. However, the shrouded build is stiffer and mechanically more reliable, as the vanes are held on both sides. If either the inner or the outer platform fails, there are better chances that the blade will still hold at the other side, which prevents it from damaging the next blade rows. These failures are more likely to occur when the stator blades are held only on one side, and they can largely offset the lower cost of the cantilevered build, by means of unexpected additional maintenance cost. In the case of axial compressors for aeronautical turboengines, it is significant that failures of compressor airfoils are among the most frequent causes of in–flight shut down, aborted take off, unscheduled engine removal, delay and cancellation (Wisler, 1998).

However, with the current preference for rather low aspect ratios, these mechanical risks can be limited and cantilevered stators can constitute a cheaper and mechanically simpler design solution.

CONCLUSIONS

The present analysis shows that shrouding stators of an axial compressor or making them cantilevered impacts differently on the overall performance. In the tested compressor, higher stall margin occurs with the cantilevered build. Conversely the work coefficient and the efficiency of the shrouded build at design conditions are higher, but this result can vary depending on specific geometrical factors, such as the size of axial gaps between stator shrouds and rotor rims.

Local details of the flow field using either stator type were well predicted with a multistage steady Navier–Stokes solver. It is the authors' view that this capability should be exploited to design more efficient rotor hub sections, taking into account the specific flow state between adjacent blade rows corresponding to either stator type.

The choice of the stator hub sealing is determined more often by mechanical and economic rather than aerodynamic issues. Manufacturing costs of a cantilevered stator stage can be about 10% lower than those of a shrouded one, but other important variables relevant to the choice, like consequences on engine direct operating and maintenance costs, vary according to the specific case.

ACKNOWLEDGEMENTS

The Authors would like to express their gratitude to the BMW ROLLS–ROYCE management and to Prof. Ennio Carnevale Dean of Engineering at the University of Florence, for encouraging and promoting this joint research activity.

REFERENCES

Arnone, A. and Benvenuti, E., 1994, "Three-Dimensional Navier-Stokes Analysis of a Two-Stage Gas Turbine," *ASME paper 94-GT-88.*

Arnone, A., Liou, M. S., and Povinelli, L. A., 1993, "Multigrid Calculation of Three-Dimensional Viscous Cascade Flows,"

Journal of Propulsion and Power, Vol. 9, No. 4, pp. 605–614.

Arnone, A. and Pacciani, R., 1995, "Three-Dimensional Viscous Analysis of Centrifugal Impellers Using the Incompressible Navier-Stokes Equations," in: *1st European Conference on Turbomachinery - Fluid Dynamic and Thermodynamic Aspects*, Erlangen, pp. 181–195.

Brankiewicz, W. S. and Hathaway, M. D., 1998, "Impact of Variable-Geometry Stator Hub Leakage in a Low Speed Axial Compressor," *ASME paper 98-GT-194*.

DUT, 1997, *Low-Speed Research Compressor Dresden*, Dresden University of Technology.

Goto, A., 1991, "Three-Dimensional Flow and Mixing in an Axial Flow Compressor with Different Rotor Tip Clearances," *ASME Paper 91-GT-89*.

Heidegger, N. J., Hall, E. J., and Delaney, R. A., 1996, "Parametrized Study of High-Speed Compressor Seal Cavity Flow," *AIAA paper*, Vol. 96-2807.

Howard, M. A., Ivey, P. C., Barton, J. P., and Young, K. F., 1994, "Endwall Effects at Two Tip Clearances in a Multistage Axial Flow Compressor With Controlled Diffusion Blading," *ASME Journal of Turbomachinery*, Vol. 116, No. 4, pp. 635–647.

Swoboda, M., Ivey, P. C., Wenger, U., and Gümmer, V., 1998, "An Experimental Examination of Cantilivered and Shrouded Stators in a Multistage Axial Compressor," *ASME paper 98-GT-282*.

Wellborn, S. R. and Okiishi, T. H., 1998, "The Influence of Shrouded Stator Cavity Flows on Multistage Compressor Performance," *ASME Paper 98-GT-12*.

Wisler, D. C., 1998, "The Technical and Economic Relevance of Understanding Blade Row Interaction Effects in Turbomachinery," in: *Blade Row Interference Effects in Axial Turbomachinery Stages*, VKI Lecture Series.